

# A Perspective on the Molecular Modeling of Electrolyte Decomposition Reactions for Solid Electrolyte Interphase Growth in Lithium-Ion Batteries

Mohammed Bin Jassar, Carine Michel, Sara Abada, Theodorus De Bruin, Sylvain Tant, Carlos Nieto-Draghi, and Stephan N. Steinmann\*

The solid electrolyte interphase (SEI) is a thin heterogeneous layer formed at the anode/electrolyte interface in lithium-ion batteries as a consequence of the reduction of the electrolyte. The initial formation of the SEI inhibits the direct contact between the electrode and the electrolyte and thus protects the battery. However, the composition, structure, and size of the SEI evolve over time and the growth of the SEI is considered the primary mechanism leading to the gradual deterioration of the battery performance. Despite the importance of the SEI and its growth, the atomistic understanding of the underlying elementary reaction steps remains partial. Molecular modeling of the electrolyte decomposition is key to gain detailed insights that are complementary to experiments for the reactions occurring in this heterogeneous interphase. In this perspective, the electron transport mechanisms are first described from the anode to the electrolyte through the SEI and highlight the importance of the inorganic/organic interface within the heterogeneous SEI: it is where the electrolyte decomposition reactions are likely to occur. Finally, a view is provided on the current progress on molecular modeling techniques (e.g., Density Functional Theory, force fields, machine learning potentials) of the SEI and the challenges each method faces.

## 1. Introduction

The solid electrolyte interphase (SEI) is a passivating layer that forms at the anode (e.g., Li-metal or Li intercalated in graphite)/electrolyte interface in lithium-ion batteries.<sup>[1–4]</sup> The electrolyte is generally composed of organic solvents (e.g., ethylene carbonate (EC)), salts (lithium hexafluorophosphate (LiPF<sub>6</sub>)), and additives (e.g., vinylene carbonate (VC)). The SEI forms as a result of the electrolyte reduction by electrons from the anode since the Fermi level of the anode is higher than the lowest unoccupied molecular orbital of the electrolyte.<sup>[1]</sup> Due to its isolating nature, the SEI largely protects the electrolyte from further reduction after the initial cycles of the battery. Nevertheless, the SEI continues to grow slowly over time, consuming active electrons and electrolyte species which leads to capacity loss and eventually the death of the battery.<sup>[5–7]</sup>

Experimental studies<sup>[5–7]</sup> have identified a multi-layered, mosaic structured SEI:<sup>[8]</sup> in

general, the SEI close to the anode is rich in dense inorganic compounds (essentially composed of Li<sub>2</sub>CO<sub>3</sub>, LiF, and Li<sub>2</sub>O) at the anode/SEI interface and an outer porous organic layer (containing mostly alkyl carbonates, polymers, etc.) at the SEI/electrolyte interface. However, the arrangement and distinction between layered and mosaic structure is not only subject to debate,<sup>[9,10]</sup> but also depends on the precise nature of the setup, e.g., working potential<sup>[11]</sup> and external pressure.<sup>[12]</sup> Furthermore, the structure and composition of both SEI layers evolve with time and space (lateral heterogeneity).<sup>[3,4]</sup> Even though experimental studies have been able to provide information about the composition of the SEI layer, deducing the thermodynamics and kinetics of elementary reaction steps in the SEI is highly challenging: Many reactions occur simultaneously, with little to no control by the setup, yielding a complex mixture that is, at the same time, the environment of subsequent reactions. Moreover, studying the calendar aging (shelf-lifetime) experimentally at room temperature would take years. Therefore, experimental studies are usually performed at elevated temperatures. However, elevated temperatures not only speed-up the reactions that would dominate the room-temperature regime, but could also open-up additional


M. Bin Jassar, S. Tant  
Stellantis Centre Technique Carrières-sous-Poissy  
Carrières-sous-Poissy 78955, France

M. Bin Jassar, C. Michel, S. N. Steinmann  
Univ Lyon  
ENS de Lyon  
CNRS

Laboratoire de Chimie UMR  
Lyon 5182, France  
E-mail: [stephan.steinmann@ens-lyon.fr](mailto:stephan.steinmann@ens-lyon.fr)

M. Bin Jassar, T. De Bruin, C. Nieto-Draghi  
IFP Energies nouvelles  
1 & 4 Av. Bois Préau, Rueil Malmaison 92852, France

S. Abada  
IFP Energies nouvelles  
Rond-Point de L'échangeur de Solaize—BP3, Solaize 69360, France

 The ORCID identification number(s) for the author(s) of this article can be found under <https://doi.org/10.1002/adfm.202313188>

© 2024 The Authors. Advanced Functional Materials published by Wiley-VCH GmbH. This is an open access article under the terms of the [Creative Commons Attribution](#) License, which permits use, distribution and reproduction in any medium, provided the original work is properly cited.

DOI: 10.1002/adfm.202313188

side-reaction channels. To complement these experimental studies, many computations have been performed on various levels (atomistic to continuum) to deepen our understanding of the decomposition reactions leading to the SEI formation and growth. In this perspective we focus on the atomistic computational studies, which still face substantial challenges that need to be overcome in order to draw reliable conclusions. But, before we can understand the SEI growth, we need to identify the main electron transport mechanisms and where electrolyte decomposition reactions take place within the complex heterogeneous SEI.

## 2. Electron Transport Mechanisms

The SEI growth is believed to be diffusion-controlled, either through electrolyte diffusion from the bulk to the SEI<sup>[13–17]</sup> or through the diffusion of electrons from the anode to the SEI. Three main electron transport mechanisms from the anode to the electrolyte can be distinguished.

- i. *Electron Tunneling*:<sup>[14,18]</sup> Electron tunneling decays exponentially with distance. Still, if the SEI layer is thin (less than 1–2 nm), electrons can tunnel from the anode through the SEI layer and reduce the electrolyte.
- ii. *Electron Conduction*:<sup>[14–16]</sup> if the SEI layer is an electronically conductive layer, electrons can be transported through the SEI.<sup>[19,20]</sup>
- iii. *Li<sup>0</sup> Diffusion*:<sup>[14,16,21–23]</sup> in this indirect electron transport mechanism, electrons from the anode combine with Li<sup>+</sup> from the SEI, leading to Li<sup>0</sup> atoms that diffuse through the SEI and ultimately react with reducible species.

It should be noted that all transport mechanisms can contribute to the SEI formation and growth with different degrees at different stages of battery aging. Now that the possible electron transport mechanisms have been presented, we will discuss the SEI multi-layer structure and its implications on the degradation reactions in more details.

## 3. Where do the Decomposition Reactions Take Place?

The electrolyte decomposition reactions take place somewhere around the SEI. Continuum models often use a plane separating two zones, namely the anode and the electrolyte to describe the SEI.<sup>[24]</sup> To reach a better comprehension, it is necessary to go beyond this simplified model. The SEI starts growing at the anode/electrolyte interface where the anode is in direct contact with the electrolyte. However, once the initial SEI has formed, it protects the electrolyte from the direct contact with the anode and two new interfaces arise: anode/SEI and SEI/electrolyte. The SEI has a mosaic, multi-layer structure,<sup>[9,10]</sup> with the long-term structure being dominated by mainly inorganic compounds closer to the anode and organics in contact with the electrolyte and solvent, see **Figure 1**. Once this multi-layered structure is generated, the electrolyte decomposition reactions could take place at three possible interfaces, as discussed below.

*Interface I*: At the anode/SEI interface the electrolyte decomposition reactions are limited by electrolyte diffusion through the

SEI until it reaches the anode surface,<sup>[13,25]</sup> see **Figure 1**. Note that the inner inorganic layer of the SEI is dense and does not allow the diffusion of electrolyte species (e.g., solvents, salts) all the way up to the anode interface,<sup>[3,4,26]</sup> unless there are mechanical cracks that are quickly healed by reactions that are analogous to the initial formation of the SEI. So, it is unlikely that we can find electrolyte species over the surface of the anode. As a consequence, the anode/SEI interface is not expected to be the interface where decomposition reactions (SEI growth) occur.

*Interface II*: At the electrolyte/SEI interface, the SEI growth is limited by electron transport through the whole SEI,<sup>[15,18,27,28]</sup> and especially through its organic outer part. The SEI organic layer is porous and contains many reducible species (e.g., solvent and salts).<sup>[3,4,26]</sup> Hence, electrons and radical species originating from the anode are unlikely to diffuse all the way until they reach the organic layer/electrolyte interface. Therefore, the decomposition reactions are not expected to occur at this interface either.

*Interface III*: At the inorganic/organic interface<sup>[29]</sup> found inside the SEI, the SEI growth may be limited either by the electron transport through the inorganic layer or/and the electrolyte species diffusion through the porous organic layer. At this interface (see **Figure 1**), the growth reactions occur over the inorganic salts. Such an “intermediate” interface was first proposed by Single et al.<sup>[16]</sup> as the main interface for SEI long-term growth, as it seems most compatible with the combined presence of solvent and “effective” electrons, i.e., Li<sup>0</sup>. In view of the generally mosaic structure (lateral heterogeneity) of the SEI,<sup>[8]</sup> this proposition needs some clarification: The Li<sup>0</sup> atoms are expected to originate from the electrode and diffuse until they reach a reducible species. In an initially mosaic SEI with reducible organic species close to the electrode, Li<sup>0</sup> is expected to increase the inorganic content.<sup>[30]</sup> At the same time, inorganic particles that have detached from the electrode and are found in the outer layer, are no longer expected to be key for the SEI growth.

Electrons can tunnel to interface II when the SEI thickness is less than 1–2 nm,<sup>[3,4,31]</sup> which corresponds to the initial moments of SEI formation. In the longer term, the inorganic layer of the SEI is composed of insulators (e.g., LiF with a band gap of 14 eV)<sup>[32]</sup> and can reach a thickness of  $\approx 30$  nm.<sup>[33,34]</sup> Hence, neither tunneling nor electron conduction up to interface II will contribute significantly to the long-term growth as confirmed by experimental impedance spectroscopy showing that electron transport through the SEI is rather limited.<sup>[19,20]</sup> In a comparative study of possible transport mechanisms, Single et al.<sup>[34]</sup> used a continuum model in comparison with experimental data.<sup>[35,36]</sup> They showed that Li<sup>0</sup> diffusion (up to interface III) is the only electron conduction mechanism that allows reproducing long-term SEI growth and corresponding capacity losses in excellent agreement with experiments.

## 4. Modeling the SEI Growth: A Brief Description of the Available Methods

SEI growth is a multiscale, multi-physics problem that can be studied in detail at a given scale or tackled by combining information gathered at different scales. Continuum 1D models have

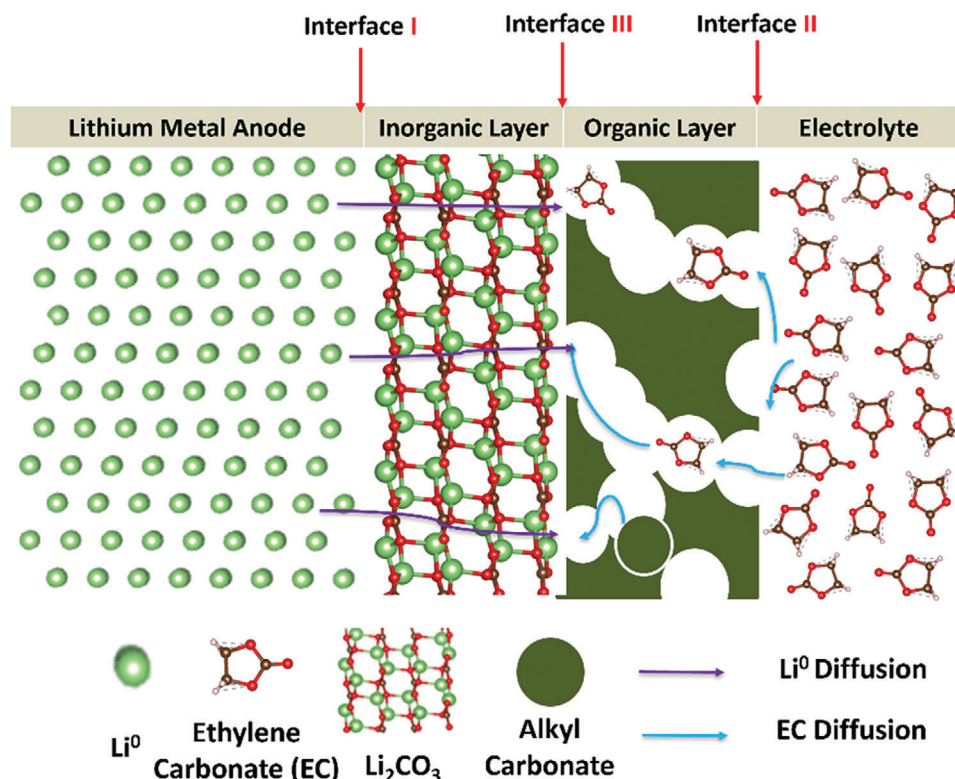


**Figure 1.** Schematic SEI structure and growth mechanism for a locally layered structure. Instead of a Li metal electrode we could also have drawn a graphitic carbon electrode with Li being intercalated as the microscopic SEI growth mechanism is similar for both architectures. For clarity only  $\text{Li}_2\text{CO}_3$  is used to represent the inorganic layer which can also be formed from  $\text{Li}_2\text{O}$  and  $\text{LiF}$ ; the electrolyte is only depicted as the solvent EC, but it also contains other species like  $\text{LiPF}_6$  salts. Reprinted (adapted) with permission from [29] Copyright 2023 American Chemical Society.

been used with success to identify transport limitations.<sup>[24,34,37]</sup> However, we will focus here on methods that can provide an atomistic view on the underlying phenomenon during the SEI growth. This refined picture might allow rationalizing the electrolyte composition and propose modifications to control the SEI growth and hence the loss in the capacity. The purpose of this section is to give a very brief overview on the different available methods and the respective merits that are summarized in Table 1. We give estimates for trajectories of  $\approx 1$  ns, a time-length that is typical to achieve equilibration at the solid/liquid interface. In bulk solution, the equilibration is 10 to 50 times faster, while amorphous systems such as the SEI have much slower overall dynamics. Additionally, it should be noted that SEI growth is a slow process (battery aging takes years). Hence enhanced sampling methods are critical (e.g., metadynamics), an aspect that is further discussed at the end of Section 5.2 together with approaches to include contributions from reaction entropies.

**Density Functional Theory:** When aiming at describing reactions (including electron transfer, bond breaking, and bond formation), first principles, quantum mechanical methods are typically used. Among them, Density Functional Theory (DFT) is today the most used method. DFT provides reactions energies and activation energies of elementary steps with a good compromise between accuracy and computational cost, including for reactions occurring at surfaces or complex interfaces. Still, compared to true “ab initio” post-Hartree-Fock methods such as coupled-cluster singles, doubles and perturbative triples, CCSD(T), DFT

has a certain “empirical” component: first, the density functional contains global (system-independent) parameters that cannot be uniquely determined from theory and, second, most DFT approximations require a “dispersion correction” which relies on empirically fitted parameters. The latter corrections are required to account for weak London-type (long-range) attraction (typically between two alkane molecules), but have also been shown to be important for medium-range interactions, e.g., even within a (branched) alkane.<sup>[38]</sup> The typical computational cost of a 1 ns trajectory for 1000 atoms can be estimated to be about 10 years, i.e., practically unfeasible today.

Atomistic simulations to describe electron tunneling are also generally performed at the DFT level for the electronic structure, with non-equilibrium Green’s functions being used to describe the actual electron transport.<sup>[39]</sup> While this method is applied on a near-routine basis for molecular electronics,<sup>[40]</sup> applications to material sciences are scarce.<sup>[41]</sup> Instead, electronic conductivities are, at best, estimated via semi-classical approaches,<sup>[42]</sup> and mostly only the spatial evolution of the electronic structure is analyzed,<sup>[43]</sup> which can be connected to simplified models for electron tunneling.<sup>[27]</sup>

**Semi-Empirical Methods:** Compared to first principles methods such as DFT and post-HF, semi-empirical methods introduce fitted (element-specific) parameters to reduce the computational cost. The most common formalism is called the neglect of diatomic differential overlap which comprises three main approximations: 1) The core electrons are not explicitly treated as they

**Table 1.** Strengths and weaknesses of various (atomistic) modeling methods going from the largest scale to the smallest one.

| Method                      | Advantages   | Disadvantages   |
|-----------------------------|--|---|
| kinetic Monte Carlo         | <ul style="list-style-type: none"> <li>- long-time scale accessible (<math>&gt;&gt; \text{ns}</math>)</li> <li>- large systems (<math>&gt;&gt; 1000</math> atoms)</li> <li>- Well adapted to amorphous systems</li> </ul>  | <ul style="list-style-type: none"> <li>- Atomistic view is lost</li> <li>- Only very approximate energy expressions</li> <li>- Accurate rate constants needed for critical steps</li> </ul> |
| Classical Force fields      | <ul style="list-style-type: none"> <li>- ns to ms time scales accessible</li> <li>- large systems (<math>&gt;&gt; 1000</math> atoms)</li> <li>- Adapted to study diffusion</li> </ul>  | <ul style="list-style-type: none"> <li>- Approximate energy functions (low accuracy)</li> <li>- Reactive events cannot be described</li> </ul>  |
| Machine-learning potentials | <ul style="list-style-type: none"> <li>- Good transferability</li> <li>- ns time scale</li> <li>- adapted for systems of <math>\approx 1000</math> atoms</li> <li>- High accuracy for energies</li> </ul>  | <ul style="list-style-type: none"> <li>- Poor transferability</li> <li>- High cost for parametrization</li> <li>- Extrapolation to new configurations is hazardous</li> </ul>               |
| Reactive force fields       | <ul style="list-style-type: none"> <li>- ns time scale</li> <li>- adapted for systems of <math>\approx 1000</math> atoms</li> <li>- Combination of diffusion and chemical reactivity can be studied</li> </ul>   | <ul style="list-style-type: none"> <li>- Difficult parametrization</li> <li>- Limited accuracy</li> <li>- Limited transferability</li> </ul>  |
| Semi-empirical methods      | <ul style="list-style-type: none"> <li>- <math>\approx 100</math> ps time scale</li> <li>- adapted for <math>\approx 1000</math> atoms</li> <li>- adapted to study reactions in disordered media via rare-events methods</li> </ul>  | <ul style="list-style-type: none"> <li>- Limited accuracy</li> <li>- Implementations are often inefficient</li> </ul>   |
| Density functional theory   | <ul style="list-style-type: none"> <li>- Good transferability</li> <li>- <math>\approx 10</math> ps time scale</li> <li>- adapted for <math>&lt; 1000</math> atoms</li> <li>- adapted to study transition states via optimizations</li> <li>- High accuracy and transferability</li> </ul> | <ul style="list-style-type: none"> <li>- High computational cost</li> </ul>   |

are assumed to be irrelevant for chemical reactivity, i.e., only valence electrons are considered in the Hamiltonian. 2) A minimal basis set is used to represent atomic orbitals. 3) The number of computed electron-electron repulsion integrals is significantly reduced, which is the main origin of the computational savings. These approximations require the introduction of parameters that are more or less transferable depending on the method and the fitting procedure. The computational cost is significantly reduced compared to first principles computations, i.e., the 1 ns trajectory for 1000 atoms would take several months.

**Reactive Force Fields:** Reactive force fields rely on distance-dependent bond orders to smoothly switch on/off the bonded terms, while the overall mathematical form closely resembles classical force fields (vide infra). Performing MD simulations with a reactive force field such as ReaxFF, yields the evolution (in

the ps to ns time scale) of a complex reactive mixture accounting for reactive events and transport limitations. However, the extent of required ab initio data and the general difficulty to ensure a good transferability from the training data set to real cases makes the parameterization of these force fields challenging. ReaxFF MD is significantly less demanding in terms of resources than DFT: a 1 ns trajectory for 1000 atoms will be rather obtained in a few days.

**Machine-Learning Potentials:** A generic mathematical expression such as a neural network can be used to construct a machine-learning potential (MLP). Most MLPs replace the physics-inspired mathematical form by a very large number of parameters (in the order of  $10^5$  to  $10^6$ ). This implies a very important parametrization effort and large amounts of training data. Furthermore, MLPs are very system specific (vide infra). Still, once



parametrized they can reach high accuracies (similar to DFT) and are computationally efficient (similar to reactive force fields).<sup>[44,45]</sup>

**Classical Force Fields:** A classical force field (FF) describes the forces between atoms using a simple mathematical expression such as harmonic springs, Coulomb interactions between fixed point charges and a Lennard-Jones-type potential for weak non-bonded interactions. These classical force fields generally lack “many-body” effects, i.e., they are pair-wise additive and are, thus, missing cooperative effects such as polarization. Furthermore, the topology (bonds) are usually predefined by the user. Force fields are generally parameterized against quantum mechanical computations or experimental data (structures for proteins, solvation, and phase-change data for solvent/solutes) if available. In combination with a classical force field, molecular dynamics (MD) can provide detailed information about the diffusion/transport of species within a liquid or a porous system of a given morphology. A 1 ns trajectory can be obtained in less than a day for a system  $\approx 1000$  atoms.

**Kinetic Monte Carlo:** kMC describes the evolution of events (e.g., reaction, diffusion) over time using parametrized rate constants of physical and chemical processes. The rate constants used in kMC can be obtained theoretically (e.g., DFT) or fitted to experiments. Due to its stochastic nature, kMC is capable of handling larger time scales than MD simulations, typically reaching seconds or even hours depending on the (relative) rate constants involved.<sup>[46,47]</sup> Reaching these larger time and length scales is achieved at the expense of the lost atomistic vision of the system under inspection. Still, the spatial and temporal distribution of species is conserved and can give feedback to smaller scales.

## 5. Atomistic Insights into the SEI Growth

### 5.1. Transport

The rate of the SEI growth is often believed to be controlled by transport, either of the electrolyte/solvent or of the reducing agent (electron or  $\text{Li}^0$ ). Shi et al.<sup>[22]</sup> were the first to propose the importance of radical  $\text{Li}^0$  diffusion using a multiscale theoretical methodology (DFT and mesoscale diffusion equations). Their results suggested that  $\text{Li}^0$  atoms diffuse through the inorganic SEI ( $\text{Li}_2\text{CO}_3$  in their case) to reach the electrolyte, where  $\text{Li}^0$  dissociates into  $\text{Li}^+$  and an electron. This mechanism was found to be compatible with the self-discharging of a lithiated electrode and/or the SEI growth.<sup>[22]</sup> Later, the existence of neutral  $\text{Li}^0$  interstitial point defect in  $\text{Li}_2\text{CO}_3$  was demonstrated by Shi et al.<sup>[23]</sup> Their DFT computations suggest that the diffusion of  $\text{Li}^0$  in  $\text{Li}_2\text{CO}_3$  requires only a small activation energy of  $\approx 0.3$  eV. Then, other SEI inorganic salts such as  $\text{LiF}$  and  $\text{Li}_2\text{O}$  were also found to be suitable for  $\text{Li}^0$  diffusion.<sup>[48]</sup> Chen et al.<sup>[49]</sup> have calculated Li migration energy barriers along the major diffusion pathways of the three main components,  $\text{LiF}$ ,  $\text{Li}_2\text{O}$ , and  $\text{Li}_2\text{CO}_3$ . Their DFT results gave energy barriers of 0.7 eV, 0.2–1.4 eV, and 0.2–0.5 eV respectively in presence of Li vacancies. Follow-up experimental and computational studies reported the diffusion coefficient of  $\text{Li}^0$  inside such inorganic layers in the range between  $(10^{-14} - 10^{-16} \text{ m}^2 \text{ s}^{-1})$ .<sup>[16,23,49–59]</sup> It should be noted that the diffusion coefficients through the inorganic SEI are generally computed assuming a prefactor of  $10^{13} \text{ s}^{-1}$  and the diffusion pathway is restricted to grain-boundaries. Hence, if the SEI is very

crystalline, such diffusion coefficients are significantly overestimated. On the other limit, i.e., when the SEI is nearly amorphous, biased MD simulations would be more appropriate than the static transition state searches to determine the (activated) diffusion events. Such simulations would have the advantage to intrinsically contain an estimate for the associated activation entropy and, thus, the prefactor (vide infra). Still, the so far computed barriers and corresponding diffusion coefficients confirm the plausibility of  $\text{Li}^0$  radicals being responsible for the long-term SEI growth. Other studies started to explore the role of the inorganic salts on the Li transport and electron-transfer properties.<sup>[54,60]</sup> For example, Kamphaus et al. used DFT to investigate the effect of salts like  $\text{Li}_2\text{O}$ ,  $\text{LiOH}$ , and  $\text{Li}_2\text{CO}_3$  on the electron transport in Li-metal batteries.<sup>[60]</sup> They found that these salts significantly slow down the charge transfer compared to pristine Li-metal.

The solvent/electrolyte diffusion through the organic layer to reach Interface II can also be critical. Using classical force fields, structural aspects<sup>[61,62]</sup> and transport properties can be assessed. For example, a MD study showed that the energy barrier of  $\text{Li}^+$  desolvation (0.4–0.5 eV) is lower than the energy barrier of  $\text{Li}^+$  transport in bulk alkyl carbonate,  $\text{Li}_2\text{BDC}$ , (0.6 eV), which shows that the transport of  $\text{Li}^+$ , not the desolvation, is the limiting step for the  $\text{Li}^+$  transport resistance.<sup>[4,62]</sup> It was also found that  $\text{Li}^+$  transport inside an organic SEI made of dilithium ethylene decarbonate ( $\text{Li}_2\text{EDC}$ ) in an ordered SEI layer is 2–3 times faster than in a disordered/amorphous layer. Furthermore,  $\text{Li}^+$  diffusion was found to depend only weakly on the temperature.<sup>[4,61,62]</sup> This highlights the importance to distinguish entropic (temperature independent) and enthalpic contributions for diffusion events.

### 5.2. Solvent Degradation

First principles computations can study the thermodynamics and kinetics of the physical and chemical processes inside the battery. DFT-based studies to investigate different pathways for electrolyte degradation started more than 20 years ago.<sup>[63,64]</sup> These studies focused on the decomposition pathways of the main solvent ethylene carbonate, as it is the most used solvent in lithium-ion batteries and forms a stable SEI when it decomposes. This decomposition has been reported to occur via two competitive mechanisms: one-electron reduction mechanism and two-electron reduction mechanism. Leung proposed a two-electron reduction mechanism that is expected to occur at the beginning of SEI formation where the anode is in direct contact with the electrolyte.<sup>[65]</sup> Similarly, the decomposition reaction of EC on Li-metal as described by grand-canonical DFT<sup>[66]</sup> is only relevant at the very first moments of the SEI formation. However, once the SEI is formed and the electrolyte is protected from the anode, the one-electron reduction mechanism becomes more likely. We refer the reader to the literature<sup>[3,4,63,65,67–71]</sup> for further details on different mechanisms and possible reaction pathways. Since the one-electron mechanism governs the battery capacity loss, we herein first summarize the most relevant corresponding studies. Second, we discuss approaches that could be applied to reach a more comprehensive and realistic understanding of these reactions.

Most DFT computations have been focusing on the reduction of EC in vacuum or simple implicit solvents in isolation, i.e., EC

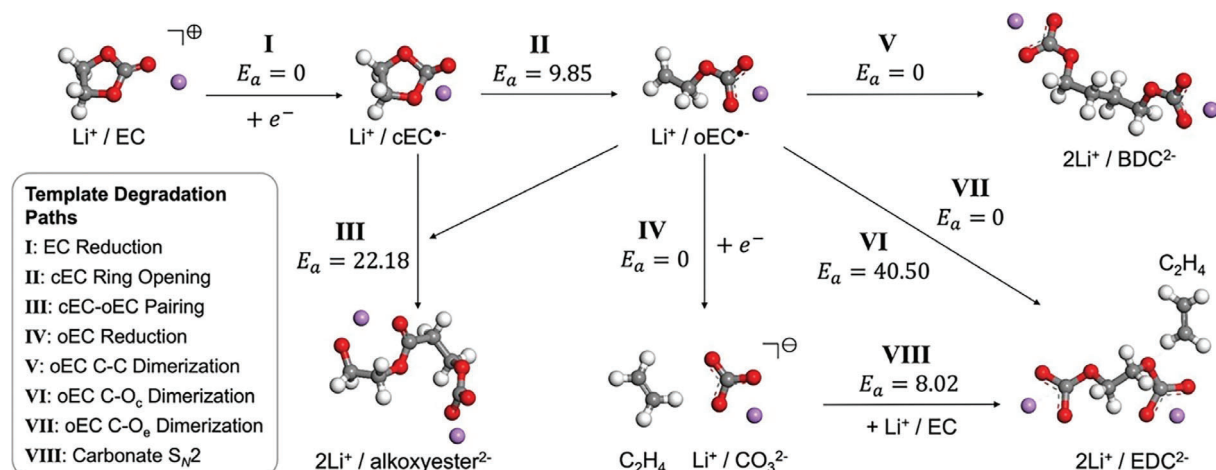


**Figure 2.** Most important reaction paths for EC decomposition with DFT electronic activation energies (in kcal mol<sup>-1</sup>) in the gas-phase. Unless stated, grouped species are charge neutral. Color code C in grey, O in red, H in white, and Li in purple. Reprinted (adapted) with permission from [67] Copyright 2022 American Chemical Society.

and Li<sup>0</sup> as reactants without complex environments<sup>[63,68,69,72,73]</sup> and determining only electronic energies, see **Figure 2** for details. Furthermore, these studies focused on single conformers, thereby neglecting conformational entropy as well. It is suggested that EC degradation starts once EC and an electron (or Li<sup>0</sup>) meet. This association (reaction I) yields, without any barrier, cLi-EC•, where “c” indicates that ethylene carbonate ring structure is still “closed” and • reminds the reader that this species is a radical. cLi-EC• can undergo ring-opening (reaction II) leading to the formation of oLi-EC•, where “o” stands for “open”. This ring-opening can start a cascade of reactions and is, therefore, critical. The cross reaction between oLi-EC• and cLi-EC• (reaction III) can lead to alkoxyesters, while, upon further reduction, oLi-EC• can also decompose into ethylene and carbonate (reaction IV). Alternatively, oLi-EC• can dimerize via C-C bond coupling, yielding dilithium butylene dicarbonate (Li<sub>2</sub>BDC), reaction V. oLi-EC• can also dimerize via C-O bond formation, leading to Li<sub>2</sub>EDC, a process that might have a barrier depending on which oxygen atom is involved in the C-O bond formation (reaction VI versus VII). Finally, Li<sub>2</sub>EDC can also be formed via reaction VIII, where carbonate is involved. As extensively discussed in the supporting information of ref.<sup>[72]</sup> standard DFT functionals can give largely varying results (up to 90 kJ mol<sup>-1</sup> difference) for even the simplest ring-opening reaction. Indeed, already 20 years ago a benchmark study found that DFT in general is not fully reliable for these one-electron reduction reactions when compared to high-level ab initio (CCSD(T)) values.<sup>[74]</sup> Hence, on the one hand the greatest care is in order not to overinterpret DFT data. Instead, whenever possible, higher-level methods should be applied, ideally exploiting embedding approaches to account for the environment. This strategy is emerging in solution chemistry,<sup>[75]</sup> but could be applied to SEI reactions. On the other hand, it also questions the use of DFT for parametrizing lower-level methods, including reactive force fields and machine-learning potentials.

Recent studies have investigated the decomposition reactions of the solvent in presence of a Li surface mimicking the Li-metal electrode<sup>[76–78]</sup> or on top of inorganic surfaces<sup>[29]</sup> to account for a more realistic reaction environment. This brings us to a more

general issue: First, from an electrochemical point of view, one would expect the electrochemical potential to play a role and, second, given the amorphous, complex structure of the SEI, disregarding entropic effects is a drastic approximation. Including the effect of the electrochemical potential over metallic electrodes can be achieved via grand-canonical DFT in combination with implicit solvent models.<sup>[79,80]</sup> This has emerged as a convenient approximation in electrocatalysis,<sup>[81]</sup> and has also been applied to reactions at the electrode of batteries.<sup>[77,82,83]</sup> However, the implicit solvent models are in principle mostly applicable to liquid electrolytes and diffuse double layers. In a (mosaic) SEI, the reaction (assumed to occur at interface III of Figure 1) is not occurring in close contact with the metallic electrode, so that the electric field can be considered screened by the (inorganic) SEI components. Moreover, due to the amorphous, slowly diffusing nature of the SEI species, it is unlikely that the SEI arranges itself in accordance with theories for diffuse double layers when Li<sup>0</sup> atoms react with organic species. The fact that the SEI is amorphous and rather solid than liquid has a significant impact on the second point: To include the effects of SEI environment more faithfully (solvent, solute, additive, and SEI species) one would need to perform a periodic boundary conditions molecular dynamics simulation to take into account the configurational/conformational entropic contributions together with the chemical reactivity. We remind the reader that the entropy ( $\Delta S^\ddagger$ ) plays a major role in the prefactor that links activation energies ( $\Delta H^\ddagger$ ) and rate constants ( $k$ ) according to Eyring's equation:

$$k = \kappa \frac{k_B T}{h} e^{\frac{\Delta S^\ddagger}{k_B}} e^{-\frac{\Delta H^\ddagger}{k_B T}} \quad (1)$$

where  $\kappa$  is the transmission coefficient,  $k_B$  Boltzmann's constant,  $T$  the temperature, and  $h$  Planck's constant.

In the gas-phase, entropic corrections can be added on a routine basis via statistical mechanics for ideal-gas, rigid-rotors, and harmonic oscillators. However, in the condensed phase<sup>[84]</sup> (and by extension in even more heterogeneous media such as the SEI), it is a huge challenge to compute or estimate entropic corrections.

In this case, only biased molecular dynamics, such as thermodynamic integrations, umbrella sampling, or metadynamics can achieve reasonable estimates. However, due to the slow dynamics and larger system size required to achieve a representative structure of the SEI, such simulations are currently absent from the literature (in contrast to biomolecular simulations<sup>[85]</sup> and, to some extent, heterogeneous catalysis)<sup>[86]</sup> but motivate the development of computationally efficient, reasonably accurate approaches, e.g. MLPs or empirical FF, to describe the relevant reactions and reaction medium.

### 5.3. Electrolyte Degradation

The electrolyte often contains fluoride-based salts,<sup>[3,4,31]</sup> which help decrease the growth of the SEI by decomposing into an insulating dense LiF layer. In particular, LiPF<sub>6</sub> is not corrosive, and allows a relatively high mobility of Li<sup>+</sup>.<sup>[31]</sup> LiF has a more negative electron affinity and hence is more effective in electron blocking (Li<sup>0</sup>) than Li<sub>2</sub>O and Li<sub>2</sub>CO<sub>3</sub>.<sup>[3,48,50,87]</sup> A DFT study comparing lithium bis(fluorosulfonyl)imide (LiFSI) and lithium bis(trifluoromethylsulfonyl)imide (LiTFSI) salts suggests that LiFSI-based electrolytes may decompose into LiF (over the surface of Li-metal anode)-containing SEIs more efficiently than LiTFSI, resulting in a more protective mechanism for the Li-metal electrode.<sup>[88]</sup> Another DFT study was performed by Di Muzio et al. to investigate the hydrolysis path for the decomposition of various salts LiPF<sub>6</sub>, LiTFSI, LiFSI and the hybrid salt lithium fluorosulfonyl-trifluoromethylsulfonyl imide.<sup>[89]</sup> They found that LiTFSI leads to more precipitation of solid LiF compared to the other electrolyte salts under these hydrolysis conditions. However, the corrosive nature of LiTFSI toward the aluminum current collector limits its uses.

Chapman et al. performed a DFT study using the cluster-continuum approach on the dissociation of common Li salts (LiTFSI, LiPF<sub>6</sub>, LiBF<sub>4</sub>, and LiClO<sub>4</sub>) in aprotic polar linear dimethyl carbonate and cyclic propylene carbonate.<sup>[90]</sup> They found that LiPF<sub>6</sub> is the most dissociated electrolyte.<sup>[90]</sup> However, LiPF<sub>6</sub> can decompose into a PF<sub>5</sub>-solvent adduct, which has a solvent-dependent stability.<sup>[91]</sup> PF<sub>5</sub> was found to be more stable in polar and sterically compact solvents such as EC than in less polar and bulky, linear carbonates such as dimethyl and diethyl carbonate.

A recent study performed by Spotte-Smith et al.<sup>[92]</sup> shows that the decomposition of the salt LiPF<sub>6</sub> is kinetically more favorable when it reacts with the inorganic species Li<sub>2</sub>CO<sub>3</sub> rather than with H<sub>2</sub>O (hydrolysis). Their results indicate that the formation of the protective LiF layer (from decomposition of LiPF<sub>6</sub>) does not necessarily depend on the presence of water but rather on the presence of the inorganic salt Li<sub>2</sub>CO<sub>3</sub>. In other words, just like for the EC reduction discussed above, the presence of the SEI is important to account for when investigating the electrolyte decomposition.

### 5.4. Organic Additives Degradation

Besides inorganic salts, organic additives are also added into the electrolyte in an attempt to tune the mechanical properties of the

organic layer of the SEI, mostly via polymer formation. These polymers are essential to form a stable (resistant to cracking) SEI layer to increase the lifetime of the battery. However, higher degrees of polymerization lead to slower diffusion kinetics and thus to longer charging times. Hence, a compromise between transport limitations and mechanical stability has to be achieved. In addition to the mechanical properties, an organic layer that is resistant to electron reduction protects the electrolyte from further reduction and hence leads to a lower capacity fade.<sup>[73]</sup> However, due to its complexity, the exact structure of the organic layer is not known yet. Recent studies started to investigate the degradation of additives to provide a deeper understanding.<sup>[73,93]</sup>

Gibson and Pfaendtner investigated the impact of additives on the SEI growth.<sup>[93]</sup> They studied the oligomerization pathways and reaction networks using DFT and semi-empirical-based molecular dynamics. They found that the additives vinyl carbonate and fluoroethylene carbonate form stable adducts with various species (e.g., oLi-EC-) via low-lying transition states, thus modifying the polymerization pathways of ethylene carbonate. A more detailed study was then performed by Kuai et al. who investigated these polymerization pathways using ab initio molecular dynamics.<sup>[73]</sup> They found that Li<sup>+</sup> acts as a catalyst for the polymerization and that the vinyl carbonate ring-opening polymerization dominates the oligomerization process. They also found that the polymerization and decomposition reactions are faster for vinyl- than for ethylene carbonate, but that their cross-coupling has an even lower activation energy. These results are in good agreement with the experimental evidence<sup>[94–96]</sup> that using vinyl carbonate as an additive enhances the battery performance.

### 5.5. Evolution of the Multiphase Structuring of the SEI

The multiphase structuring of the SEI results from the evolution of a complex mixture (solvent, electrolyte, organic additives) in contact with the anode. To embrace such a complexity, reactive force fields are generally used. A study by Bedrov et al. has developed a ReaxFF parameterization to reproduce the ring-opening reaction of cLi-EC-,<sup>[70]</sup> see Figure 3a. Later, Islam et al. developed “eReaxFF” to investigate competitive decomposition pathways.<sup>[71,97]</sup> Without going into the details, in eReaxFF the valence electron of Li is treated explicitly in a pseudo-classical manner. The developed force field predicted results for the ethylene carbonate decomposition reactions in good agreement with the reference data available in the literature.<sup>[63]</sup> Furthermore, the MD simulations were able to describe the reduction mechanism of EC, the ring opening of cLi-EC-, and subsequent radical termination reactions at elevated temperatures (600 K), see Figure 3b. However, the localization of the electron in all species was different from spin density obtained with DFT,<sup>[63]</sup> questioning the physically correct description of the reactivity of these molecules. A study by Takenaka et al. used a ReaxFF to investigate the SEI growth for a ≈1 mol L<sup>-1</sup> LiPF<sub>6</sub> EC-based electrolyte and a lithiated graphite electrode through a hybrid molecular dynamics, Monte-Carlo simulation.<sup>[98]</sup> They predicted a possible SEI structure, see Figure 3c. However, their model neither includes polymerization reactions nor the effect of the inorganic layer on the electron-transfer rate. In another study, Xie et al. performed a joint ReaxFF-DFT multi-scale simulation to investigate the initial



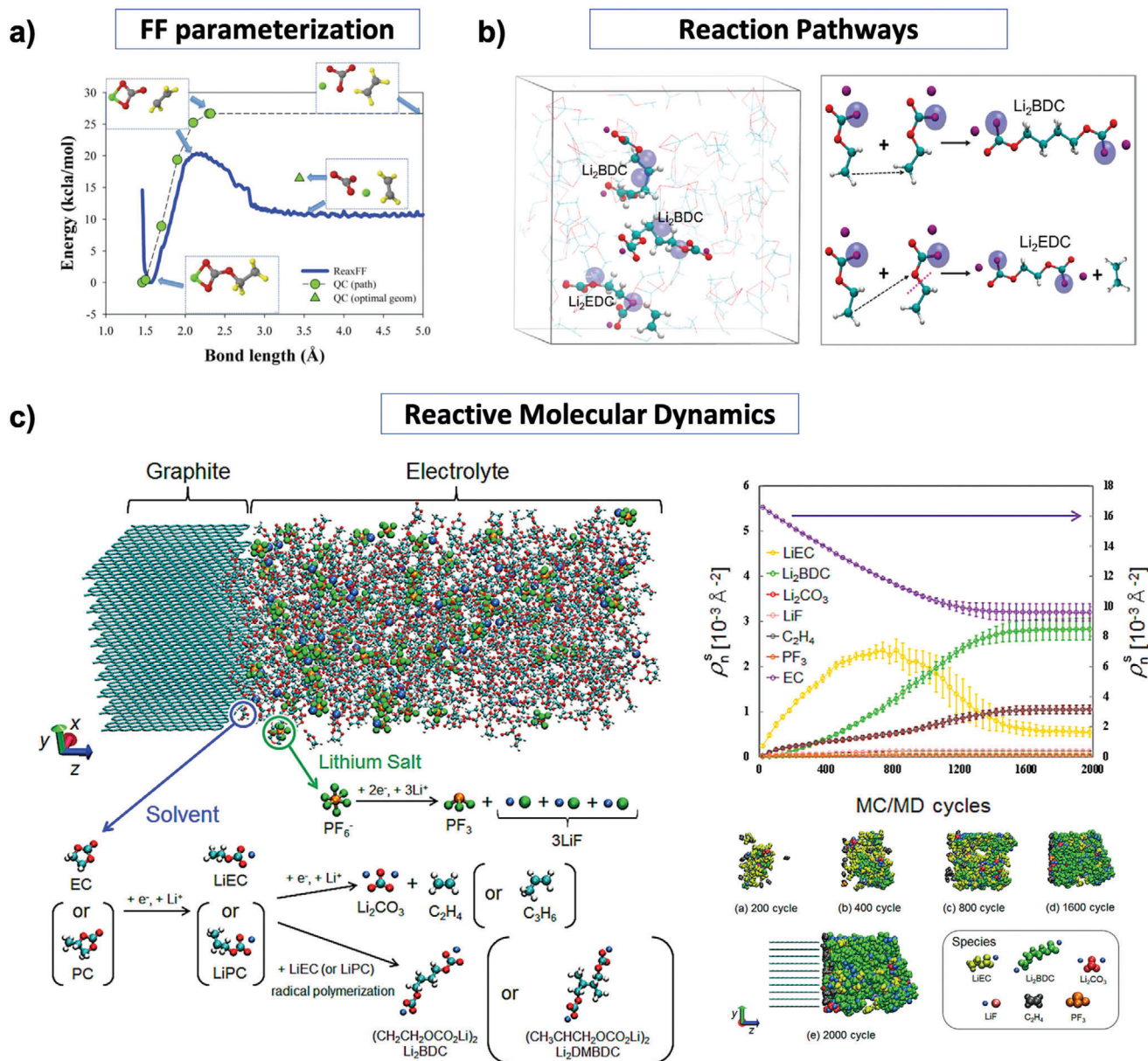


**Figure 3.** a) Comparison between DFT computations (green points) and ReaxFF (blue lines), showing reasonable agreement for the formation of ethylene from oLi-EC. Reprinted (adapted) with permission from [70] Copyright 2012 American Chemical Society b) Reactive events observed by eReaxFF molecular dynamics simulations (120 ps at 600 K) showing the formation of  $\text{Li}_2\text{BDC}$ ,  $\text{Li}_2\text{EDC}$ , and  $\text{C}_2\text{H}_4$  starting from 60 EC molecules and 40 Li atoms. Delocalization of the explicit electrons (blue spheres) can occur during the MD. Reprinted (adapted) with permission from [71] Copyright 2016 American Chemical Society c) (left) Model system of the SEI growth over a lithiated graphite electrode in a  $\approx 1 \text{ M LiPF}_6$  EC-based electrolyte via a hybrid MD/MC simulation and the considered reaction scheme. (right top) evolution of the number densities of the solvent and reaction products during the SEI formation as a function of the MC/MD cycles (right, bottom) Five snapshots of the SEI structural evolution during the hybrid MC/MD reaction simulation. Reprinted (adapted) with permission from [98] Copyright 2014 American Chemical Society.

reactions of  $1.0 \text{ mol L}^{-1} \text{ LiPF}_6$  salt in 1,3-dioxolane.[99] They found that  $\text{PF}_5$  formed from  $\text{LiPF}_6$  decomposition can initiate the polymerization of 1,3-dioxolane. The resulting polymer might enhance the mechanical stability of the Li electrode.[99]

Another way to embrace a large number of possible reactions and species is to set up a kMC model. For instance, Methekar et al. developed a kMC model to study the formation of the SEI on a graphite surface.[100] They found that the time required

for charging the battery decreases with the number of cycles due to the growth of the passive SEI layer and the concomitant capacity loss.[100] Another kMC model was developed by Hao et al. to investigate the growth of the SEI at a graphite electrode during charging.[53] The parameters were taken from previous experimental and theoretical studies.[23,101] They found that the SEI thickness and the charging time depend on the activation energy for  $\text{Li}^+$  diffusion through the SEI. As this activation



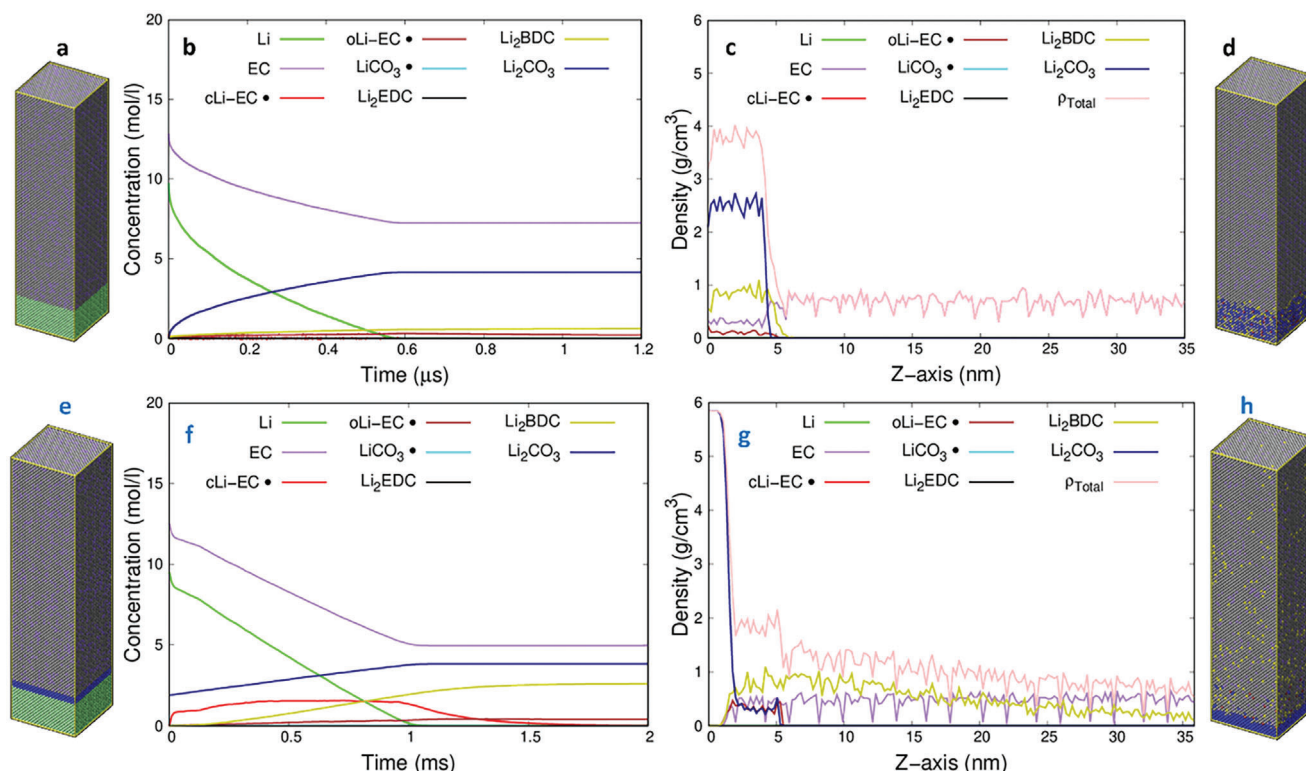


**Figure 4.** Results of kMC simulations for the formation and evolution of the SEI, formally starting from metallic lithium (green) and EC as a solvent (purple/grey). a–d) Results for rate constants for the EC decomposition reactions that have been computed in isolation: a) Initial conditions b) Variation of the concentration of species versus time c) Final specific mass density profile along the Z-axis of the simulation box d) Snapshot of the simulation box after 0.6  $\mu$ s. e–h) Results for rate constants for EC decomposition reactions that have been computed over  $\text{Li}_2\text{CO}_3$  (001): e) Initial conditions f) Variation of the concentration of species versus time g) Final specific mass density profile along the Z-axis of the simulation box h) Snapshot of the simulation box after 1.2 ms.  $\rho_{\text{total}}$  is the total density. Reprinted (adapted) with permission from<sup>[29]</sup> Copyright 2023 American Chemical Society.

energy increases, the SEI thickness increases and the charging time decrease.<sup>[4,53]</sup> Their results highlight the importance of the description of the porous nature of the SEI to understand the diffusion of electrolyte species. Other MC-based studies focused on the effect of temperature on the lithium reduction rate and SEI thickness.<sup>[4]</sup> It was found that as temperature increases, the lithium reduction rate decreases, leading to an increase in total charging time.<sup>[4]</sup> Furthermore, an increased temperature also speeds up solvent diffusion and, thus, the SEI thickness increases.

Other recent studies focused on exploiting DFT and MD/MC in multi-level simulations to model SEI growth. A study by Abbott et al. carried out EC decomposition reaction in vacuum in isolation to obtain activation energies and reaction energies to be used later in a kinetically corrected MC-MD simulations to study the SEI growth. They predicted a multilayered SEI structure.<sup>[67]</sup> Another study by Spotte-Smith et al. also studied EC degradation reactions.<sup>[72]</sup> They performed DFT calculations to obtain rate constants/activation energies to be used in a 1D kMC model to study the growth of the SEI. Their model also predicted a multilayered SEI structure.<sup>[72]</sup> In our own recent study,<sup>[29]</sup> we have used a DFT-kMC approach to investigate the main reactions leading to the formation of the SEI as well as the effect of the inorganic salts (e.g.,  $\text{Li}_2\text{CO}_3$  as interface III in Figure 1) on the kinetics of the SEI growth and capacity loss (i.e.,  $\text{Li}^0$  loss). We

found that the decomposition reactions of EC in the absence of inorganic salts (in isolation) mostly lead to the formation of inorganic species and a non-linear loss of  $\text{Li}^0$ /capacity over time, see Figure 4a–d. However, reactions occurring over the inorganic salt  $\text{Li}_2\text{CO}_3$  led to the slower formation of a more realistic SEI multilayered structure: inorganic species ( $\text{Li}_2\text{CO}_3$ ) close to the anode and organic species ( $\text{Li}_2\text{BDC}$ ) close to the interface with the electrolyte. Furthermore, reactions over  $\text{Li}_2\text{CO}_3$  led to a linear behavior of  $\text{Li}^0$ /capacity loss over time, see Figure 4e–h. Overall, our study predicted a shift from a nonlinear to a linear behavior for the capacity loss induced by SEI growth over time in agreement with previous experimental and theoretical studies. By comparison with  $\text{Li}_2\text{O}$  (111), which could form from the decomposition of  $\text{Li}_2\text{CO}_3$ , we found that the selectivity of the decomposition reactions of EC forming the SEI strongly depends on the nature of the inorganic surface which could explain the complex heterogeneous composition of the SEI. This study also highlights a major limitation: the time-scales (sub-seconds) are very far from being realistic (the corresponding reactions take years to go to completion in experiments). Among several approximations, the oversimplified estimation of rate constant prefactors, i.e., entropic contributions, might be most severe: It is very likely that the reorganization of the complex environment (and the associated entropic cost) slows down the reaction rates compared to the simple estimates.

## 6. Developing Reliable, Fast, and Easy to Parametrize Energy Expressions for Atomistic SEI Models

As presented above, DFT and reactive force fields are the most popular energy expressions for atomistic modeling of SEI-related reactions. Here, we discuss two alternatives to achieve simulations with a lower computational cost than DFT: (i) Machine-learning potentials which come with the promise that they reach DFT accuracy at much lower cost and (ii) semi-empirical methods which are similarly transferable as DFT and are still computationally much more efficient.

### 6.1. Machine Learning Potentials

Machine learning potentials are heavily parametrized mathematical functions that are used to predict the interatomic energy at a computational cost that is low compared to electronic structure computations such as DFT but that achieves a comparable accuracy.<sup>[7,64]</sup> The current state-of-the-art underlying machine-learning frameworks that can handle complex chemical systems (e.g., SEI) include Gaussian process-based learning,<sup>[102]</sup> neural network potentials,<sup>[103]</sup> and graph neural networks.<sup>[104,105]</sup> Details about the different ML-based models are out of the scope of this perspective, but are treated in dedicated reviews<sup>[7,64,106]</sup> which discuss the potential of using ML-based models for SEI systems. Rather, we discuss major concerns and challenges regarding the development of machine-learning potentials in the context of reactions in the SEI.

Machine-learned potentials are based on the hypothesis that correlations between the atomic structure and corresponding forces and energies are sufficient to parametrize very general mathematical expressions that do not contain any physics-inspired functional forms. To achieve this ambitious goal, descriptors (e.g., geometric fingerprints, graphs) are used to map the atomic coordinates and the chemical identity of the atoms into a transferable description of the system.<sup>[107]</sup> For given systems (constant stoichiometry, limited reactivity), the mathematical flexibility is currently sufficient to reach an accuracy comparable between MLP and DFT, sometimes even surpassing the latter, if sufficient high-level *ab initio* data is available for the training. The best documented example for this case is chemistry of neutral, closed-shell organic molecules.<sup>[108]</sup> Note, however, the restriction: These highly accurate MLPs are generally neither applicable to radicals nor to (de-)protonated forms. Still, sacrificing some accuracy, a partial extension can be achieved to cations and anions.<sup>[109]</sup> The absence of physics inspired functional forms is at the heart of the limitation of machine-learned potentials when it comes to extrapolations, i.e., to chemical systems that are “unlike” the ones that have been used to parametrize the model. For instance, a parametrization for ethylene carbonate is not transferable to vinyl carbonate, even though the two molecules share many common features.

Machine-learned potentials suffer from the lack of transferability since they are trained by using a specific training set and the mathematical description is even less adapted to extrapolations compared to force fields. This makes studying a new SEI system with a new electrolyte slow and expensive.<sup>[110]</sup> Furthermore, most

machine-learned potentials are unable to properly deal with long-range electron transfer reactions and the electrochemical potential in general.<sup>[7,64,111]</sup> In practice, the development of these potentials heavily relies on the relevance of the available DFT reference data. In particular, all potential reactants, products, intermediates and transition states should be included. However, most intermediates and reaction pathways to build the reference data for SEI system are yet unknown, especially when considering the reaction medium and not idealized situations in the gas-phase.

The use of autonomous reaction explorer models<sup>[112]</sup> can help to map out large SEI reaction networks.<sup>[64,107,110]</sup> Active learning models, relying on query by committee like DeePMD-kit<sup>[113]</sup> can also help construct the training sets needed on the fly, i.e., it would explore the chemical space at the same time as the model gets parametrized.<sup>[107]</sup> Similarly, reinforcement learning<sup>[114]</sup> can also help to identify reaction paths for electrolyte degradation. For example, Lan et al. have successfully exploited reinforcement learning to predict the lowest energy pathway for the Haber-Bosch reaction over Fe (111),<sup>[114]</sup> suggesting that such an approach could yield precious insights for the SEI growth.

### 6.2. Semi-Empirical Methods as a Compromise

Despite fundamental limitations of current density functionals due to the delocalization error,<sup>[115]</sup> DFT provides a convenient framework and generally useful accuracy for studying the reactivity in the SEI. However, DFT is computationally expensive and remains limited to systems of around 1000 atoms. This size is not sufficient to achieve a representative description of the amorphous SEI. Low-cost electronic structure methods (semi-empirical methods) can be used as a faster alternative to DFT. Semi-empirical methods are parametrized approximations to DFT or Hartree-Fock,<sup>[116–119]</sup> i.e., they can describe bond-formation and charge-transfer events based on quantum mechanics. Common semi-empirical methods are PM7,<sup>[117]</sup> density functional tight binding (DFTB)<sup>[120–125]</sup> and GFN2-xtb.<sup>[119]</sup> The underlying parameters are determined via specific training sets from experimental and/or higher-level theoretical data. As a consequence, their performance also depends on the quality and relevance of the training set used. In the context of SEI system, Li et al. developed a Self-Consistent Charge DFTB parameters for Li–Li, Li–H, Li–O, Li–C using DFT reference data.<sup>[126]</sup> The developed method was then used to model the Li<sup>+</sup> desolvation energy and the diffusion coefficient in liquid ethylene carbonate and was able to capture the effect of SEI thickness in blocking the electron transfer for Li/Li<sub>2</sub>CO<sub>3</sub>/liquid-EC. However, the training set used to develop these parameters neither included fluorinated compounds (e.g., LiPF<sub>6</sub>) nor the major solvent decomposition reaction energies (e.g., the formation of organic alkyl carbonates, polymers, etc.). The inclusion of these reactions in future training sets would be important to model the electrolyte decomposition reactions with more confidence. Other DFTB-based methods were developed by Grimme and co-workers, dubbed GFN-xtb and GFN2-xtb.<sup>[118,119]</sup> Those methods use mainly global and element-specific parameters and avoid the pair-specific potentials of standard DFTB. We very recently have performed a benchmark study<sup>[127]</sup> of the semi-empirical methods GFN-xtb, GFN2-xtb, PM6-D3, and PM7-D3 to investigate their performance to

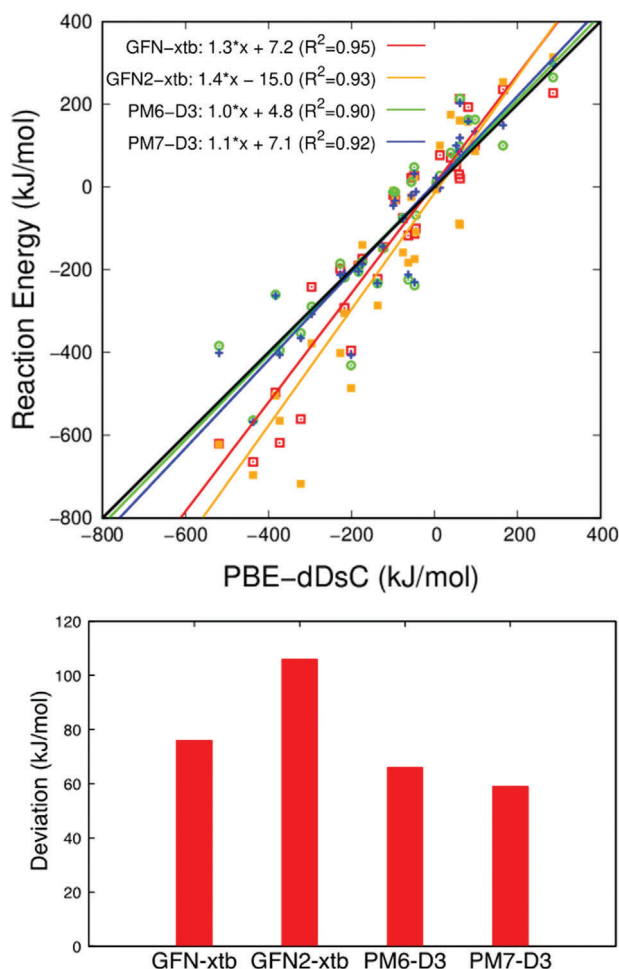


**Figure 5.** Top: Parity plot of four semi-empirical methods (GFN-xtb, GFN2-xtb, PM6-D3, and PM7-D3) against DFT (PBE-dDsC) for the 32 model reactions related to the SEI formation and growth. The reactions include oxidation of Li atoms, acid-base reactions, carbon radical formation, propagation, and termination reactions among others. Bottom: The mean absolute deviation of these methods against DFT (PBE-dDsC). Reprinted (adapted) with permission from [127]. Copyright 2024 American Chemical Society.

model 32 SEI reactions including the decomposition of major electrolyte species of solvents, salt, and additives. **Figure 5** shows a parity plot of the four semi-empirical methods against DFT (PBE-dDsC) and their corresponding values of the mean absolute deviations (MADs). The slope of both PM6-D3 and PM7-D3 is closer to unity in comparison to GFN-xtb and GFN2-xtb, suggesting that PM6-D3 and PM7-D3 feature a smaller systematic error. PM7-D3 was also found to have the lowest MAD ( $59 \text{ kJ mol}^{-1}$ ) and worked satisfactorily well within a wide range of reactions and systems, including nanoparticles of inorganic salts.

The interaction between the inorganic and organic species of the SEI is still rarely addressed in the literature. Semi-empirical methods are computationally efficient enough to perform molecular dynamics simulations of such systems, e.g. inorganic nanoparticles ( $\text{Li}_2\text{CO}_3$ , LiF,  $\text{Li}_2\text{O}$ ) in contact with various organic species (EC,  $\text{Li}_2\text{EDC}$ ,  $\text{Li}_2\text{BDC}$ ). MD simulations at 300 K reveal a high reactivity of the nanoparticle  $\text{Li}_2\text{O}$  which led to the de-

composition of the organic species ( $\text{CO}_2$  dissociation for  $\text{Li}_2\text{EDC}$  and  $\text{Li}_2\text{BDC}$ ; ring-opening and deprotonation of EC). However, for two other salts, LiF and  $\text{Li}_2\text{CO}_3$ , the organic species were stably adsorbed on the surface of the nanoparticle. Assuming the organics from the electrolyte decomposition reactions form at least a mono-layer of strongly adsorbed, non-reducible species over the inorganic layer, they can be seen as a passivating layer blocking reducible electrolyte species to come close to the surface of the inorganic layer and thereby hindering their reduction by  $\text{Li}^0$ . Thereby, the organic SEI might also slow down the kinetics of SEI growth and capacity loss. To clarify these hypotheses, we recommend investigating the activation energy and rate constants of the desorption of organic species, e.g.,  $\text{Li}_2\text{BDC}$  over the inorganic solids (e.g.,  $\text{Li}_2\text{CO}_3$ ,  $\text{Li}_2\text{O}$ ) and their reactivity with  $\text{Li}^0$  at the interface.

Given the applicability of PM7-D3 and GFN-xtb to the entire periodic table, this reasonable accuracy of the two methods for reactions occurring in the SEI provides opportunities for in-depth studies of interfaces and reactivities that have been difficult to model with DFT beyond the prototypical case of the Li-ion batteries, such as Si-modified Li-metal electrodes<sup>[128]</sup> or to investigate the atomistic origin of the pressure dependence of the SEI-formation.<sup>[12]</sup> Nevertheless, to reach a higher level of confidence in the results, reweighting methods<sup>[129,130]</sup> exploiting a higher-level of theory such as DFT<sup>[131]</sup> or even post-HF,<sup>[75]</sup> should be used in a second step.

## 7. Conclusion and Outlook

The SEI is a heterogeneous layer that forms at the electrode/electrolyte interface in lithium-ion batteries. The SEI has a multi-layered, mosaic structure: an inorganic-rich layer near the electrode and an outer organic-rich layer near the electrolyte. Based on a critical analysis of the literature and the physical chemistry of the SEI growth, the chemical reactions pertaining to the SEI growth should take place over the inorganic layer that is in contact with the electrode on the one side and with the organic layer on the other side. Hence, the inclusion of the inorganic layer in determining the electrolyte decomposition kinetics is essential to better describe the kinetics of SEI growth and hence capacity loss. This implies on the one hand that explicit electrochemical potential effects are largely screened by the inorganic layer, i.e., that the reactivity is expected to be different compared to the one in a typical electrochemical double layer over a metallic electrode. On the other hand, activation (free) energies for elementary reactions should take the complex environment into account to include entropic contribution appropriately. Indeed, configurational and conformational entropy cost of local rearrangements of the SEI to let the reactions occur are likely to be important. The determination of the activation free energies in the SEI is one of the formidable tasks that will have to be tackled via biased molecular dynamics simulations. Similarly, the reactions and activated diffusion in solid-state-electrolytes have to be addressed with equivalent methods, as they are even less likely to be well represented by implicit solvation models.

DFT-based methods have been able to provide insights on the initial moment of the electrolyte degradation. Still, when compared to high-level ab initio methods such as CCSD(T), the

accuracy of these DFT results is debatable and, with the advent of embedding and reweighting methods, the use of beyond-DFT methods should increase dramatically. Furthermore, DFT with non-equilibrium Green's functions is the method of choice to determine the electron transfer mechanism across various components of the SEI and their interfaces. While currently absent in the literature, we expect that the battery community will soon adopt the corresponding tools that are routinely used in molecular electronics. However, the current DFT-based methods cannot perform large-scale simulations of inhomogeneous, non-crystalline systems such as the SEI. Due to their lower computational cost, semi-empirical methods, along with reactive force fields and machine learning potentials, could be potential alternatives. Still, extensive and computationally expensive parameterization and benchmarking are needed to assess their performance against DFT. The DFT training and validation data need to include decomposition reactions pathways, reactants, products, intermediates, and transition states, including the effect of the environment, i.e., the organic and inorganic components of the SEI.

Semi-empirical methods have the advantage of capturing the most important of the quantum effects that are neglected in most force fields and machine-learned potentials, i.e., charge transfer and the peculiar reactivity of radicals. However, reaching high accuracy with semi-empirical methods remains a formidable task and they remain slower than force fields as they require the diagonalization of a Hamiltonian matrix. Compared to machine-learned potentials, reactive force fields are more physics-inspired, making them somewhat more transferable, but still less than semi-empirical methods. The use of methods like query by committee, or generally active and reinforcement learning could accelerate the development of training sets to make machine-learned potentials more accessible, although still at a high computational cost. Future developments can be foreseen in combining the best of machine-learning models and semi-empirical methods: semi-empirical models are physics inspired and, therefore, quite transferable. They also come along with a well-defined electronic structure, i.e., the electrochemical potential and charge-transfer events are properly taken into account. However, this transferability comes at the cost of a generally lower accuracy compared to DFT or machine-learned potentials: The universal parameters in the semi-empirical methods are not able to describe the fine details of individual systems. Therefore, a promising approach would be to use machine-learning to make the physical parameters of semi-empirical methods system dependent. This is, indeed, an approach that is being explored, e.g., for DFTB.<sup>[132]</sup>

In view of the success of semi-empirical methods and machine-learned potentials, we do not expect reactive force fields to increase in popularity for describing the chemistry in the SEI: their parametrization is more system-specific than semi-empirical methods and, still, they are generally less accurate than machine-learned potentials. In contrast, classical (i.e., non-reactive) force fields will continue to play a significant role in this area: their computational speed is unparalleled (and impossible to beat keeping an all-atom description) and they are ideally suited to study transport, including activated diffusion, of species across the SEI. Furthermore, with limited parametrization effort, they can already give qualitative insights of the structuring of the

inorganic/organic interface, which is identified as key in this perspective.

Kinetic Monte Carlo is proposed as the best adapted framework for studying the long-term and large-scale spatio-temporal evolution of the SEI with near-atomistic resolution. However, such simulations critically rely on the preliminary identification of the most relevant reaction steps using first-principles and semi-empirical methods. Once the reactions have been identified, environment dependent rate constants have to be determined by reliable and realistic atomistic simulations via biased molecular dynamics. For computational efficiency's sake – and avoiding time-consuming system-specific parametrization – the method of choice for reactive, large-scale biased molecular dynamics is, in our opinion, a semi-empirical method such as PM7-D3 or GFN-xtb or the above mentioned DFTB derivative.<sup>[132]</sup> These biased MD simulations will constitute a major advancement in our understanding of the reaction mechanism that drive the long-term growth of the SEI.

In summary, a better molecular understanding of electrolyte decomposition reactions would further our understanding of the SEI growth and capacity loss of lithium-ion batteries. This molecular understanding could ultimately lead to the design of better batteries. However, the main challenge facing our atomistic understanding of the SEI growth is the lack of fast *and* accurate simulation methods that describe the complex nature of this interphase including the effect of solvents, salts, and additives.

## Acknowledgements

This work was supported by the program Conventions Industrielles de Formation par la Recherche (CIFRE) N° 2020/0918 of the Association Nationale de la Recherche et de la Technologie (ANRT). The authors thank the SYSPROD project and AXELERA Pôle de Compétitivité for financial support (PSMN Data Center).

## Conflict of Interest

The authors declare no conflict of interest.

## Keywords

DFT, decomposition reactions, Li-Batteries, molecular modeling, SEI

Received: October 24, 2023

Revised: February 15, 2024

Published online:

- [1] J. B. Goodenough, Y. Kim, *Chem. Mater.* **2010**, 22, 587.
- [2] S. J. An, J. Li, C. Daniel, D. Mohanty, S. Nagpure, D. L. Wood, *Carbon* **2016**, 105, 52.
- [3] A. Wang, S. Kadam, H. Li, S. Shi, Y. Qi, *npj Comput Mater* **2018**, 4, 15.
- [4] A. A. Franco, A. Rucci, D. Brandell, C. Frayret, M. Gaberscek, P. Jankowski, P. Johansson, *Chem. Rev.* **2019**, 119, 4569.
- [5] S. Koohi-Fayegh, M. A. Rosen, J. *Energy Storage* **2020**, 27, 101047.
- [6] X. Han, L. Lu, Y. Zheng, X. Feng, Z. Li, J. Li, M. Ouyang, *eTransportation* **2019**, 1, 100005.



- [7] H. Adenusi, G. A. Chass, S. Passerini, K. V. Tian, G. Chen, *Adv. Energy Mater.* **2023**, 13, 2203307.
- [8] E. Peled, D. Golodnitsky, G. Ardel, *J. Electrochem. Soc.* **1997**, 144, L208.
- [9] Y. Li, W. Huang, Y. Li, A. Pei, D. T. Boyle, Y. Cui, *Joule* **2018**, 2, 2167.
- [10] V. R. Rikka, S. R. Sahu, A. Chatterjee, P. V. Satyam, R. Prakash, M. S. R. Rao, R. Gopalan, G. Sundararajan, *J. Phys. Chem. C* **2018**, 122, 28717.
- [11] S.-Y. Sun, N. Yao, C.-B. Jin, J. Xie, X.-Y. Li, M.-Y. Zhou, X. Chen, B.-Q. Li, X.-Q. Zhang, Q. Zhang, *Angew. Chem., Int. Ed.* **2022**, 61, 202208743.
- [12] W. Liu, Y. Luo, Y. Hu, Z. Chen, Q. Wang, Y. Chen, N. Iqbal, D. Mitlin, *Adv. Energy Mater.* **2024**, 14, 2302261.
- [13] M. B. Pinson, M. Z. Bazant, *J. Electrochem. Soc.* **2012**, 160, A243.
- [14] M. Tang, S. Lu, J. Newman, *J. Electrochem. Soc.* **2012**, 159, A1775.
- [15] F. Single, B. Horstmann, A. Latz, *Phys. Chem. Chem. Phys.* **2016**, 18, 17810.
- [16] F. Single, B. Horstmann, A. Latz, *J. Electrochem. Soc.* **2017**, 164, E3335.
- [17] R. Cappabianca, P. Angelis, M. Fasano, E. Chivazzo, P. Asinari, *Energies* **2023**, 16, 5003.
- [18] D. Li, D. Danilov, Z. Zhang, H. Chen, Y. Yang, P. H. L. Notten, *J. Electrochem. Soc.* **2015**, 162, A858.
- [19] W. Hu, Y. Peng, Y. Wei, Y. Yang, *J. Phys. Chem. C* **2023**, 127, 4465.
- [20] P. Lu, C. Li, E. W. Schneider, S. J. Harris, *J. Phys. Chem. C* **2014**, 118, 896.
- [21] F. A. Soto, Y. Ma, J. M. La Martinez de Hoz, J. M. Seminario, P. B. Balbuena, *Chem. Mater.* **2015**, 27, 7990.
- [22] S. Shi, P. Lu, Z. Liu, Y. Qi, L. G. Hector, H. Li, S. J. Harris, *J. Am. Chem. Soc.* **2012**, 134, 15476.
- [23] S. Shi, Y. Qi, H. Li, L. G. Hector, *J. Phys. Chem. C* **2013**, 117, 8579.
- [24] C. Edouard, M. Petit, C. Forgez, J. Bernard, R. Revel, *J. Power Sources* **2016**, 325, 482.
- [25] H. J. Ploehn, P. Ramadass, R. E. White, *J. Electrochem. Soc.* **2004**, 151, A456.
- [26] A. A. Franco, *RSC Adv.* **2013**, 3, 13027.
- [27] Y.-X. Lin, Z. Liu, K. Leung, L.-Q. Chen, P. Lu, Y. Qi, *J. Power Sources* **2016**, 309, 221.
- [28] C. D. Quilty, D. Wu, W. Li, D. C. Bock, L. Wang, L. M. Housel, A. Abraham, K. J. Takeuchi, A. C. Marschillok, E. S. Takeuchi, *Chem. Rev.* **2023**, 123, 1327.
- [29] M. Bin Jassar, C. Michel, S. Abada, T. De Bruin, S. Tant, C. Nieto-Draghi, S. N. Steinmann, *ACS Appl. Energy Mater.* **2023**, 6, 6934.
- [30] E. Peled, D. Golodnitsky, C. Menachem, D. Bar-Tow, *J. Electrochem. Soc.* **1998**, 145, 3482.
- [31] B. Philippe, Insights in Li-ion Battery Interfaces through Photoelectron Spectroscopy Depth Profiling, Acta Universitatis Upsaliensis, Uppsala, 1041, **2013**.
- [32] P. Mazur, L. Markowski, M. Grodzicki, *Vacuum* **2009**, 84, 622.
- [33] B. Han, Z. Zhang, Y. Zou, K. Xu, G. Xu, H. Wang, H. Meng, Y. Deng, J. Li, M. Gu, *Adv. Mater.* **2021**, 33, 2100404.
- [34] F. Single, A. Latz, B. Horstmann, *ChemSusChem* **2018**, 11, 1950.
- [35] P. Keil, A. Jossen, *J. Electrochem. Soc.* **2016**, 164, A6066.
- [36] P. Keil, S. F. Schuster, J. Wilhelm, J. Travi, A. Hauser, R. C. Karl, A. Jossen, *J. Electrochem. Soc.* **2016**, 163, A1872.
- [37] L. Kolzenberg, A. Latz, B. Horstmann, *ChemSusChem* **2020**, 13, 3901.
- [38] S. N. Steinmann, M. Wodrich, C. Corminboeuf, *Theor. Chem. Acc.* **2010**, 127, 429.
- [39] N. Papior, N. Lorente, T. Frederiksen, A. García, M. Brandbyge, *Comput. Phys. Commun.* **2017**, 212, 8.
- [40] S. Y. Quek, K. H. Khoo, *Acc. Chem. Res.* **2014**, 47, 3250.
- [41] D. Stradi, N. R. Papior, O. Hansen, M. Brandbyge, *Nano Lett.* **2017**, 17, 2660.
- [42] G. K. H. Madsen, J. Carrete, M. J. Verstraete, *Comput. Phys. Commun.* **2018**, 231, 140.
- [43] Y. Ren, J. Liu, C. Zhang, H. Zhuang, C. Sun, G. Cai, X. Tan, S. Sun, *Chem. Eng. J. Adv.* **2022**, 12, 100377.
- [44] Y. Zuo, C. Chen, X. Li, Z. Deng, Y. Chen, J. Behler, G. Csányi, A. V. Shapeev, A. P. Thompson, M. A. Wood, S. P. Ong, *J. Phys. Chem. A* **2020**, 124, 731.
- [45] P. S. Rice, Z.-P. Liu, P. Hu, *J. Phys. Chem. Lett.* **2021**, 12, 10637.
- [46] A. A. Franco, Y. Yin, In *Encyclopedia of Interfacial Chemistry*, Elsevier, New York **2018**, pp. 739.
- [47] F. Röder, R. D. Braatz, U. Krewer, *J. Electrochem. Soc.* **2017**, 164, E3335.
- [48] K. Leung, K. L. Jungjohann, *J. Phys. Chem. C* **2017**, 121, 20188.
- [49] Y. C. Chen, C. Y. Ouyang, L. J. Song, Z. L. Sun, *J. Phys. Chem. C* **2011**, 115, 7044.
- [50] A. Ramasubramanian, V. Yurkiv, T. Foroozan, M. Ragone, R. Shahbazian-Yassar, F. Mashayek, *J. Phys. Chem. C* **2019**, 123, 10237.
- [51] H. Schranzhofer, J. Bugajski, H. J. Santner, C. Korepp, K.-C. Möller, J. O. Besenhard, M. Winter, W. Sitte, *J. Power Sources* **2006**, 153, 391.
- [52] M. D. Levi, C. Wang, D. Aurbach, Z. Chvoj, *J. Electroanal. Chem.* **2004**, 562, 187.
- [53] F. Hao, Z. Liu, P. B. Balbuena, P. P. Mukherjee, *J. Phys. Chem. C* **2017**, 121, 26233.
- [54] H. Yildirim, A. Kinaci, M. K. Y. Chan, J. P. Greeley, *ACS Appl. Mater. Interfaces* **2015**, 7, 18985.
- [55] H. Iddir, L. A. Curtiss, *J. Phys. Chem. C* **2010**, 114, 20903.
- [56] N. A. Kaskhedikar, J. Maier, *Adv. Mater.* **2009**, 21, 2664.
- [57] P. G. Kitz, M. J. Lacey, P. Novák, E. J. Berg, *J. Power Sources* **2020**, 477, 228567.
- [58] K. Hayamizu, *J. Chem. Eng. Data* **2012**, 57, 2012.
- [59] P. Guan, L. Liu, X. Lin, *J. Electrochem. Soc.* **2015**, 162, A1798.
- [60] E. P. Kamphaus, S. Angarita-Gomez, X. Qin, M. Shao, M. Engelhard, K. T. Mueller, V. Murugesan, P. B. Balbuena, *ACS Appl. Mater. Interfaces* **2019**, 11, 31467.
- [61] D. Bedrov, O. Borodin, J. B. Hooper, *J. Phys. Chem. C* **2017**, 121, 16098.
- [62] O. Borodin, D. Bedrov, *J. Phys. Chem. C* **2014**, 118, 18362.
- [63] Y. Wang, S. Nakamura, M. Ue, P. B. Balbuena, *J. Am. Chem. Soc.* **2001**, 123, 11708.
- [64] D. Diddens, W. A. Appiah, Y. Mabrouk, A. Heuer, T. Vegge, A. Bhowmik, *Adv. Materials Inter* **2022**, 9, 2101734.
- [65] K. Leung, *Chem. Phys. Letters* **2013**, 568, 1.
- [66] N. G. Hörmann, O. Andreussi, N. Marzari, *J. Chem. Phys.* **2019**, 150, 041730.
- [67] J. W. Abbott, F. Hanke, *J. Chem. Theory Comput.* **2022**, 18, 925.
- [68] J. Zhang, J. Yang, L. Yang, H. Lu, H. Liu, B. Zheng, *Mater. Adv.* **2021**, 2, 1747.
- [69] Y. Wang, Y. Liu, Y. Tu, Q. Wang, *J. Phys. Chem. C* **2020**, 124, 9099.
- [70] D. Bedrov, G. D. Smith, A. C. T. van Duin, *J. Phys. Chem. A* **2012**, 116, 2978.
- [71] M. M. Islam, A. C. T. van Duin, *J. Phys. Chem. C* **2016**, 120, 27128.
- [72] E. W. C. Spotte-Smith, R. L. Kam, D. Barter, X. Xie, T. Hou, S. Dwaraknath, S. M. Blau, K. A. Persson, *ACS Energy Lett.* **2022**, 7, 1446.
- [73] D. Kuai, P. B. Balbuena, *ACS Appl. Mater. Interfaces* **2022**, 14, 2817.
- [74] Y.-K. Han, S. U. Lee, *Theor. Chem. Acc.* **2004**, 112, 106.
- [75] J. M. P. Martinez, E. A. Carter, *J. Am. Chem. Soc.* **2023**, 145, 12561.
- [76] W. Xu, X. Liao, W. Xu, C. Sun, K. Zhao, Y. Zhao, C. Hu, *Nano Energy* **2021**, 88, 106237.
- [77] N. Lespes, J.-S. Filhol, *J. Chem. Theory Comput.* **2015**, 11, 3375.
- [78] A. Hagopian, J. Touja, N. Louvain, L. Stievano, J.-S. Filhol, L. Monconduit, *ACS Appl. Mater. Interfaces* **2022**, 14, 10319.
- [79] C. D. Taylor, S. A. Wasileski, J.-S. Filhol, M. Neurock, *Phys. Rev. B* **2006**, 73, 165402.

- [80] K. Letchworth-Weaver, T. A. Arias, *Phys. Rev. B* **2012**, *86*, 075140.
- [81] N. Abidi, K. R. G. Lim, Z. W. Seh, S. N. Steinmann, *WIREs Comput Mol Sci* **2021**, *11*, e1499.
- [82] A. Kopač Lautar, J. Bitenc, T. Rejec, R. Dominko, J.-S. Filhol, M.-L. Doublet, *J. Am. Chem. Soc.* **2020**, *142*, 5146.
- [83] A. Hagopian, M.-L. Doublet, J.-S. Filhol, *Energy Environ. Sci.* **2020**, *13*, 5186.
- [84] C. Peter, C. Oostenbrink, A. van Dorp, W. F. van Gunsteren, *J. Chem. Phys.* **2004**, *120*, 2652.
- [85] H. A. L. Filipe, M. Javanainen, A. Salvador, A. M. Galvão, I. Vattulainen, L. M. S. Loura, M. J. Moreno, *J. Chem. Theory Comput.* **2018**, *14*, 3840.
- [86] G. Collinge, S. F. Yuk, M.-T. Nguyen, M.-S. Lee, V.-A. Glezakou, R. Rousseau, *ACS Catal.* **2020**, *10*, 9236.
- [87] Z. Liu, Y. Qi, Y. X. Lin, L. Chen, P. Lu, L. Q. Chen, *J. Electrochem. Soc.* **2016**, *163*, A592.
- [88] L. E. Camacho-Forero, T. W. Smith, P. B. Balbuena, *J. Phys. Chem. C* **2017**, *121*, 182.
- [89] S. Di Muzio, A. Paolone, S. Brutti, *J. Electrochem. Soc.* **2021**, *168*, 100514.
- [90] N. Chapman, O. Borodin, T. Yoon, C. C. Nguyen, B. L. Lucht, *J. Phys. Chem. C* **2017**, *121*, 2135.
- [91] K. Tasaki, K. Kanda, S. Nakamura, M. Ue, *J. Electrochem. Soc.* **2003**, *150*, A1628.
- [92] E. W. C. Spotte-Smith, T. B. Petrocelli, H. D. Patel, S. M. Blau, K. A. Persson, *ACS Energy Lett.* **2023**, *8*, 347.
- [93] L. D. Gibson, J. Pfaendtner, *Phys. Chem. Chem. Phys.* **2020**, *22*, 21494.
- [94] D. Y. Wang, N. N. Sinha, J. C. Burns, C. P. Aiken, R. Petibon, J. R. Dahn, *J. Electrochem. Soc.* **2014**, *161*, A467.
- [95] Y. Jin, N.-J. H. Kneusels, P. C. M. M. Magusin, G. Kim, E. Castillo-Martínez, L. E. Marbella, R. N. Kerber, D. J. Howe, S. Paul, T. Liu, C. P. Grey, *J. Am. Chem. Soc.* **2017**, *139*, 14992.
- [96] Y. Jin, N.-J. H. Kneusels, L. E. Marbella, E. Castillo-Martínez, P. C. M. M. Magusin, R. S. Weatherup, E. Jónsson, T. Liu, S. Paul, C. P. Grey, *J. Am. Chem. Soc.* **2018**, *140*, 9854.
- [97] M. M. Islam, G. Kolesov, T. Verstraelen, E. Kaxiras, A. C. T. van Duin, *J. Chem. Theory Comput.* **2016**, *12*, 3463.
- [98] N. Takenaka, Y. Suzuki, H. Sakai, M. Nagaoka, *J. Phys. Chem. C* **2014**, *118*, 10874.
- [99] M. Xie, Y. Wu, Y. Liu, P. P. Yu, R. Jia, W. A. Goddard, T. Cheng, *Mater. Today Energy* **2021**, *21*, 100730.
- [100] R. N. Methekar, P. W. C. Northrop, K. Chen, R. D. Braatz, V. R. Subramanian, IEEE, San Francisco, CA, pp. 1512–1517.
- [101] O. Borodin, G. V. Zhuang, P. N. Ross, K. Xu, *J. Phys. Chem. C* **2013**, *117*, 7433.
- [102] A. P. Bartók, M. C. Payne, R. Kondor, G. Csányi, *Phys. Rev. Lett.* **2010**, *104*, 136403.
- [103] J. Behler, M. Parrinello, *Phys. Rev. Lett.* **2007**, *98*, 146401.
- [104] K. T. Schütt, H. E. Sauceda, P.-J. Kindermans, A. Tkatchenko, K.-R. Müller, *J. Chem. Phys.* **2018**, *148*, 241722.
- [105] T. Xie, J. C. Grossman, *Phys. Rev. Lett.* **2018**, *120*, 145301.
- [106] N. Yao, X. Chen, Z.-H. Fu, Q. Zhang, *Chem. Rev.* **2022**, *122*, 10970.
- [107] S. N. Steinmann, A. Hermawan, M. Bin Jassar, Z. W. Seh, *Chem Catalysis* **2022**, *2*, 940.
- [108] J. S. Smith, B. T. Nebgen, R. Zubatyuk, N. Lubbers, C. Devereux, K. Barros, S. Tretiak, O. Isayev, A. E. Roitberg, *Nat. Commun.* **2019**, *10*, 2903.
- [109] R. Zubatyuk, J. S. Smith, B. T. Nebgen, S. Tretiak, O. Isayev, *Nat. Commun.* **2021**, *12*, 4870.
- [110] S. N. Steinmann, Q. Wang, Z. W. Seh, *Mater. Horiz.* **2022**, *10*, 393.
- [111] S. N. Steinmann, Z. W. Seh, *Nat. Rev. Mater.* **2021**, *6*, 289.
- [112] M. Bergeler, G. N. Simm, J. Proppe, M. Reiher, *J. Chem. Theory Comput.* **2015**, *11*, 5712.
- [113] H. Wang, L. Zhang, J. Han, W. E., *Comput. Phys. Commun.* **2018**, *228*, 178.
- [114] T. Lan, Q. An, *J. Am. Chem. Soc.* **2021**, *143*, 16804.
- [115] A. J. Cohen, P. Mori-Sanchez, W. Yang, *Science* **2008**, *321*, 792.
- [116] J. J. P. Stewart, *J. Mol. Model.* **2007**, *13*, 1173.
- [117] J. J. P. Stewart, *J. Mol. Model.* **2013**, *19*, 1.
- [118] S. Grimme, C. Bannwarth, P. Shushkov, *J. Chem. Theory Comput.* **2017**, *13*, 1989.
- [119] C. Bannwarth, S. Ehlert, S. Grimme, *J. Chem. Theory Comput.* **2019**, *15*, 1652.
- [120] Q. Cui, M. Elstner, E. Kaxiras, T. Frauenheim, M. Karplus, *J. Phys. Chem. B* **2001**, *105*, 569.
- [121] M. Elstner, D. Porezag, G. Jungnickel, J. Elsner, M. Haugk, T. Frauenheim, S. Suhai, G. Seifert, *Phys. Rev. B* **1998**, *58*, 7260.
- [122] M. Gaus, Q. Cui, M. Elstner, *J. Chem. Theory Comput.* **2012**, *7*, 931.
- [123] T. A. Niehaus, S. Suhai, F. D. Sala, P. Lugli, M. Elstner, G. Seifert, T. Frauenheim, *Phys. Rev. B* **2001**, *63*, 085108.
- [124] T. Frauenheim, G. Seifert, M. Elstner, T. Niehaus, C. Köhler, M. Amkreutz, M. Sternberg, Z. Hajnal, A. Di Carlo, S. Suhai, *J. Phys.: Condens. Matter* **2002**, *14*, 3015.
- [125] Y. Yang, H. Yu, D. York, Q. Cui, M. Elstner, *J. Phys. Chem. A* **2007**, *111*, 10861.
- [126] Y. Li, Y. Qi, *J. Phys. Chem. C* **2018**, *122*, 10755.
- [127] M. Bin Jassar, C. Michel, S. Abada, T. De Bruin, S. Tant, C. Nieto-Draghi, S. N. Steinmann, *J. Phys. Chem. C* **2024**, *128*, 3269.
- [128] Z. Chen, A. Soltani, Y. Chen, Q. Zhang, A. Davoodi, S. Hosseinpour, W. Peukert, W. Liu, *Adv. Energy Mater.* **2022**, *12*, 2200924.
- [129] E. C. Dybeck, G. König, B. R. Brooks, M. R. Shirts, *J. Chem. Theory Comput.* **2016**, *12*, 1466.
- [130] G. Lazzari, H. Jung, P. G. Bolhuis, R. Covino, *J. Chem. Theory Comput.* **2023**, *19*, 9060.
- [131] M. Sharma, M. Sierka, *J. Chem. Theory Comput.* **2022**, *18*, 6892.
- [132] G. Fan, A. McSloy, B. Aradi, C.-Y. Yam, T. Frauenheim, *J. Phys. Chem. Lett.* **2022**, *13*, 10132.